Investigations of Gravity-Driven Two-Phase Debris Flows

Xiannan Meng and Yongqi Wang

Technische Universität Darmstadt, Darmstadt 64287, Germany
{meng,wang}@fdy.tu-darmstadt.de

Abstract. A depth-integrated theory is derived for the gravity-driven two-phase debris flows over complex shallow topography. The mixture theory is adopted to describe the mass and momentum conservation of each phase. The model employs the Mohr-Coulomb plasticity for the solid rheology, and assumes the Newtonian fluid for the fluid phase. The interactive forces assumed here consist of viscous drag force linear to velocity difference between the both phases, and buoyancy force. The well-established governing equations are built in 3D topography; as a result, they are expressed in the curvilinear coordinate system. Considering the characteristics of flows, a shallow layer assumption is made to simplify the depth-integrated equations. The final resulting equations are solved numerically by a high-resolution TVD scheme. The dynamic behaviors of the mixture are investigated. Numerical results indicate that the model can adequately describe the flows of dry granular material, the pure water and general two-phase debris flows.

Keywords: mixture theory, mohr-Coulomb plasticity, newtonian fluid, high-resolution TVD scheme.

1 Introduction

Gravity-driven flows of dense sediment-fluid mixture with free surface occur commonly on the Earths surface with devastating consequences. There is a significant need for reliable models for predicting the dynamics, runout distances, and deposited areas of such events.

With respect to the modelings, three kinds of typical depth-integrated models so far exist: (i) the model of single phase dry cohesionless granular continuum consisting of particles with a nominal mean, representative size, (ii) quasi-single phase model treating the mixture as a medium combing the contributions of the fluid pressure with those from granular friction, and (iii) two-fluid model fully taking into account the interactive forces between the fluid phase and the granular phase.

The single phase model postulates that the rapidly moving granular material is density preserving and satisfies Mohr-Coulomb friction rheology. Supposing blunt velocity profile, a depth-average is performed to derive the final mass and momentum conservation equations without loosing accuracy ([2], [3], [7] and [9]).

W. Wu (ed.), *Recent Advances in Modeling Landslides and Debris Flows*,
Springer Series in Geomechanics and Geoengineering, DOI: 10.1007/978-3-319-11053-0_11

For the quasi-single phase model, the role of pore fluid is fully taken into account, and the momentum equation containing solid stress and fluid partial stress, is formulated for the mixture as a whole. Despite the fact of good agreement between the numerical results from quasi-single phase model and experimental results, the following weaknesses have to be mentioned. Firstly, the spatial and temporal distributions of the volume fractions cannot be determined due to the assumption of equality of the velocities of the two constituents. Secondly, the transport equation for the fluid pressure is postulated by means of experimental results. It lacks a theoretical justification.

Taking into account difference of velocities of all phases, the two-fluid model describes each phase in its own conservation equations. The interactive forces are assumed to couple the two sets of conservation equations. The temporal and spatial distributions of volume fractions can be obtained and analyzed (see [4, 5, 6]).

The present proposed model, based on two-fluid model and incorporating the advantages of the existing models, presents a depth-integrated theory for the two-phase debris flows over 3D shallow topography. The granular phase is modeled by Mohr-Coulomb plasitcity, and the fluid phase is modeled by Newtonian fluid. The interactive forces consist of viscous drag force and buoyancy force. A friction boundary condition is applied to constrain the basal movement of the fluid phase instead of the no-slip boundary condtion (see [6]). Like the previous works, the depth integration is performed, and a shallow layer assumption is made to simplify the governing equations. The resulting non-linear PDEs are solved by a high-resolution scheme taking into account all important effects. Through the analysis of numerical results, some important phenomena are found.

2 Governing Equations and Coordinate System

2.1 Governing Equations

In the framework of the mixture theory, all phases are present at each point of the field with different volume fractions. For each phase, the mass and momentum balance equations are postulated. Through the interactive forces, they are coupled with each other. The conservation equations for mass are given by

$$\partial_t(\widetilde{\rho}_s\phi_s) + \nabla\cdot(\widetilde{\rho}_s\phi_s\boldsymbol{u}_s) = 0, \tag{1}$$

$$\partial_t(\widetilde{\rho}_f\phi_f) + \nabla\cdot(\widetilde{\rho}_f\phi_f\boldsymbol{u}_f) = 0, \tag{2}$$

and for momentum by

$$\partial_t(\widetilde{\rho}_s\phi_s\boldsymbol{u}_s) + \nabla\cdot(\widetilde{\rho}_s\phi_s\boldsymbol{u}_s\boldsymbol{u}_s) = \nabla\cdot\hat{\boldsymbol{T}}_s + \widetilde{\rho}_s\phi_s\boldsymbol{g} + \boldsymbol{f}_s, \tag{3}$$

$$\partial_t(\widetilde{\rho}_f\phi_f\boldsymbol{u}_f) + \nabla\cdot(\widetilde{\rho}_f\phi_f\boldsymbol{u}_f\boldsymbol{u}_f) = \nabla\cdot\hat{\boldsymbol{T}}_f + \widetilde{\rho}_f\phi_f\boldsymbol{g} - \boldsymbol{f}_s, \tag{4}$$

where the true densities and velocities of the two phases are characterized by $\widetilde{\rho}_{s/f}$ and $\boldsymbol{u}_{s/f}$. ϕ_s and ϕ_f denote the volume fractions of the granular phase and the fluid phase, respectively. $\hat{\boldsymbol{T}}_s$ and $\hat{\boldsymbol{T}}_f$ are chosen as the partial stresses of the

granular phase and the fluid phase. The gravity acceleration is denoted by $\boldsymbol{g}$. $\boldsymbol{f}_s$ is used to represent the interactive forces exerted on the granular phase by the fluid phase.

For the granular phase, we assume $\hat{\boldsymbol{T}}_s = -\phi_s \widetilde{\boldsymbol{T}}_s$, where $\widetilde{\boldsymbol{T}}_s$ is the Coulomb stress tensor for the dry granular material from the work of [9]. For the fluid phase, the relation $\hat{\boldsymbol{T}}_f = -p\boldsymbol{I} + \phi_f \widetilde{\boldsymbol{\tau}}_f$ is assumed, where p is the pressure of the fluid phase and $\widetilde{\boldsymbol{\tau}}_f$ is the shear stress of the pure fluid. In the present investigation, a Newtonian fluid is assumed.

Usually, as in [5], the interactive forces are simply assumed to be composed of the viscous drag force, which has linear relationship with relative velocity expressed as $\beta(\boldsymbol{u}_f - \boldsymbol{u}_s)$, and the buoyancy force expressed as $-\phi_s \nabla p$ (see [1]) in the present model. The coefficient of the viscous drag force β follows the expression of [8], based on the experimental data $\beta = \frac{\phi_s \phi_f (\widetilde{\rho}_s - \widetilde{\rho}_f) g}{v_T (1-\phi_s)^m}$. Here V_T is the sedimentation velocity of a single particle, and $m \in [0.39, 2.65]$ is a parameter depending on the particle Reynolds number $Re_p = \frac{v_T \, d \, \widetilde{\rho}_f}{\mu}$ (d is the diameter of the sphere particle, and μ is the viscosity of the fluid).

Finally the momentum conservation equations are rewritten in the forms:

$$\partial_t(\widetilde{\rho}_s \phi_s \boldsymbol{u}_s) + \nabla \cdot (\widetilde{\rho}_s \phi_s \boldsymbol{u}_s \boldsymbol{u}_s) = -\nabla \cdot (\phi_s \widetilde{\boldsymbol{T}}_s) + \widetilde{\rho}_s \phi_s \boldsymbol{g} - \phi_s \nabla p + \boldsymbol{f}_d, \quad (5)$$

$$\partial_t(\widetilde{\rho}_f \phi_f \boldsymbol{u}_f) + \nabla \cdot (\widetilde{\rho}_f \phi_f \boldsymbol{u}_f \boldsymbol{u}_f) = -\phi_f \nabla p + \nabla \cdot (\phi_f \widetilde{\boldsymbol{\tau}}_f) + \widetilde{\rho}_f \phi_f \boldsymbol{g} - \boldsymbol{f}_d. \quad (6)$$

As illustrated in [2], the granular phase satisfies kinematic boundary condition and stress-free dynamic boundary condition on the free surface, and the Coulomb friction boundary condition

$$\hat{\boldsymbol{T}}_s \boldsymbol{n}_b - (\boldsymbol{n}_b \cdot \hat{\boldsymbol{T}}_s \boldsymbol{n}_b)\boldsymbol{n}_b = \frac{\boldsymbol{u}_s^b}{|\, \boldsymbol{u}_s^b \,|} (\boldsymbol{n}_b \cdot \hat{\boldsymbol{T}}_s \boldsymbol{n}_b) \tan\delta, \quad (7)$$

and no-penetration boundary condition in the tangential and normal direction of the basal topography, respectively. Here $\boldsymbol{n}_b$ denotes the normal unit vector of the basal topography, and δ represents Coulomb bed friction angle.

For the fluid phase, besides the kinematic boundary condition and stress-free condition on the free surface and impermeability on the bottom, a friction law linear to its velocity is imposed on the bottom,

$$\hat{\boldsymbol{T}}_f \boldsymbol{n}_b - (\boldsymbol{n}_b \cdot \hat{\boldsymbol{T}}_f \boldsymbol{n}_b)\boldsymbol{n}_b = -k_l \boldsymbol{u}_f, \quad (8)$$

where k_l represents the friction coefficient depending on the roughness of the slope and the viscosity of the fluid etc. $k_l \to \infty$ corresponds to a no-slip condition.

2.2 Coordinate System

An orthogonal curvilinear coordinate system, $Oxyz$, is introduced by a two dimensional reference surface that follows the mean down-slope chute topography. The x-axis is oriented in the down-slope direction, the y-axis lies in the cross-slope direction of the reference surface without lateral variation, and the z-axis

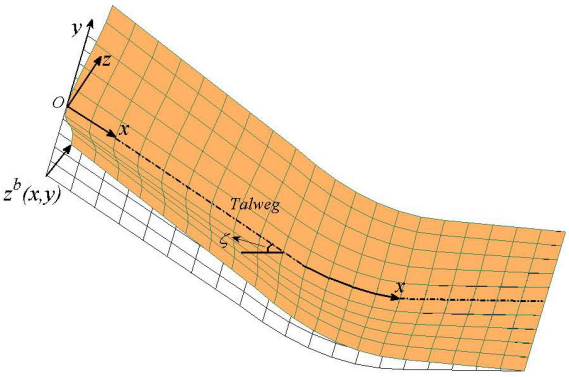

Fig. 1. Curvilinear coordinate system

is normal to them. The down-slope inclination angle of the reference surface ζ changes as a function of the down-slope coordinate x. Its gradient along x-axis is defined by $\kappa = -\frac{d\zeta}{dx}$ representing the curvature of the reference surface, where the negative sign is imposed to guarantee positive value for κ. The complex shallow three-dimensional basal topography is defined by its elevation $z = z^b(x, y)$ above the reference surface as illustrated in Fig. 1.

Following the theory of tensor and [2], the gradient of a scalar field F, the divergences of a vector field $\boldsymbol{l}$ and a symmetry second-order tensor $\boldsymbol{N}$ can be represented in terms of the contravariant components. The gradient of a vector field $\boldsymbol{l}$, which emerges in the present model due to the Newtonian shear stress for the fluid phase, but not

$$\begin{aligned}\nabla \boldsymbol{l} = &\left(\partial_x l_x - \frac{\kappa_{,x} z}{1-\kappa z} l_x - \kappa l_z\right)(1-\kappa z)\boldsymbol{e}_1\boldsymbol{e}_1 + (\partial_x l_y)(1-\kappa z)\boldsymbol{e}_1\boldsymbol{e}_2 \\ &+ (\partial_x l_z + \kappa l_x)(1-\kappa z)\boldsymbol{e}_1\boldsymbol{e}_3 + (\partial_y l_x)\boldsymbol{e}_2\boldsymbol{e}_1 + (\partial_y l_y)\boldsymbol{e}_2\boldsymbol{e}_2 + (\partial_y l_z)\boldsymbol{e}_2\boldsymbol{e}_3 \\ &+ \left(\partial_z l_x - \frac{\kappa}{1-\kappa z} l_x\right)\boldsymbol{e}_3\boldsymbol{e}_1 + (\partial_z l_y)\boldsymbol{e}_3\boldsymbol{e}_2 + (\partial_z l_z)\boldsymbol{e}_3\boldsymbol{e}_3, \end{aligned} \tag{9}$$

where $\boldsymbol{e}_1$, $\boldsymbol{e}_2$ and $\boldsymbol{e}_3$ are unit base vectors along x-, y- and z-axis, respectively.

3 Scaling Analysis

The scaling analysis is performed with the equations:

$$\begin{aligned} &(x, y, z, t) = (Lx^*, Ly^*, Hz^*, \sqrt{L/g}t^*), \\ &\kappa = \frac{1}{\mathcal{R}}\kappa^*, \\ &((u, v, w)\mid_{f,s}, v_T) = \sqrt{gL}((u^*, v^*, \epsilon w^*)\mid_{f,s}, \epsilon v_T^*), \\ &(\widetilde{T}_{s(xx)}, \widetilde{T}_{s(yy)}, \widetilde{T}_{s(zz)}, p) = \widetilde{\rho}_s g H(\widetilde{T}^*_{s(xx)}, \widetilde{T}^*_{s(yy)}, \widetilde{T}^*_{s(zz)}, \gamma p^*), \\ &(\widetilde{T}_{s(xy)}, \widetilde{T}_{s(xz)}, \widetilde{T}_{s(yz)}) = \widetilde{\rho}_s g H \tan\delta(\widetilde{T}^*_{s(xy)}, \widetilde{T}^*_{s(xz)}, \widetilde{T}^*_{s(yz)}), \end{aligned} \tag{10}$$

where the superscript "$*$" represents dimensionless variables, which will be dropped in the following to simplify the notation. γ represents the ratio of the fluid density to the solid density. The scale for the true stress of the granular phase is introduced in accordance with Coulomb rheology (normal and shear stress are scaled with $\widetilde{\rho}_s gH$ and $\widetilde{\rho}_s gH \tan\delta$, where δ is Coulomb bed frictional angle). Two non-dimensional parameters arise due to the scaling. The aspect ratio ϵ is expressed by the typical depth of debris flows H over the typical extent L,

$$\epsilon = \frac{H}{L}, \tag{11}$$

and a characteristic curvature λ is expressed as follows,

$$\lambda = \frac{L}{\mathcal{R}}, \tag{12}$$

where $\mathcal{R}$ is typical radius of curvature.

4 Order Arguments and Depth Integration

In this section, we focus on the evolution of the depth-integrated equations for the two phases. Here we will not present the entire calculation, but only indicate the most important steps. Taking into account the flow characteristics, the 'thin layer' approximation is made that the typical down- and cross-slope lengths are much larger than the typical normal thickness, i.e. $\epsilon \ll 1$. Furthermore, following [3], $\lambda = O(\epsilon^{\alpha})$ and $\tan\delta = O(\epsilon^{\beta})$ with $0 < \alpha, \beta < 1$ are assumed.

4.1 Depth-Integrated for the Fluid Phase

Using the orthogonal coordinates displayed in Fig. 1, and with a scaling analysis as in [7], the contributions of the shear stress for the fluid phase in the down-slope, cross-slope and normal components become

$$f_x(\widetilde{\tau}_f) = \frac{\epsilon}{N_R}\left[2\frac{\partial^2 u_f}{\partial x^2} + \frac{\partial}{\partial y}\left(\frac{\partial v_f}{\partial x} + \frac{\partial u_f}{\partial y}\right) + \frac{1}{\epsilon^2}\frac{\partial^2 u_f}{\partial z^2}\right] + O(\epsilon^{1+\chi}), \tag{13}$$

$$f_y(\widetilde{\tau}_f) = \frac{\epsilon}{N_R}\left[2\frac{\partial^2 v_f}{\partial y^2} + \frac{\partial}{\partial x}\left(\frac{\partial v_f}{\partial x} + \frac{\partial u_f}{\partial y}\right) + \frac{1}{\epsilon^2}\frac{\partial^2 v_f}{\partial z^2}\right] + O(\epsilon^{1+\chi}), \tag{14}$$

$$f_z(\widetilde{\tau}_f) = O(\epsilon^{1+\chi}), \tag{15}$$

where $\chi = \min(\alpha, \beta)$. The dimensionless variable N_R is expressed as $N_R = \frac{\widetilde{\rho}_f H\sqrt{gL}}{\phi_f \mu}$, and its order is $10^5 \sim 10^6$. Similarly, the friction boundary condition for the fluid phase subject to the simplification of thin layer becomes

$$\frac{\partial u_f^b}{\partial z} = \vartheta u_f^b + O(\epsilon^2), \qquad \text{at the bottom} \quad z = b(x, y), \tag{16}$$

$$\frac{\partial v_f^b}{\partial z} = \vartheta v_f^b + O(\epsilon^2), \qquad \text{at the bottom} \quad z = b(x, y), \tag{17}$$

where $\vartheta = \frac{k_l H}{\phi_f \mu}$ is a non-dimensional parameter combing frictional coefficient, typical thickness, fluid volume fraction with fluid viscosity.

As usual, it follows from the vertical momentum equation of the fluid phase that the hydrostatic pressure is

$$p(x, y, z, t) = (s - z)\cos\zeta + O(\epsilon^{\alpha}), \tag{18}$$

where $z = s(x, y, t)$ is the free surface.

The integration is performed for the fluid momentum equations in x- and y-direction along the depth direction from the topography $z = b(x, y)$ to the free surface $z = s(x, y, t)$. In it, the mean value of any quantity $q(x, y, z, t)$ is defined as follows

$$\frac{1}{h}\int_{b(x,y)}^{s(x,y,t)} q(x, y, z, t)dz = \overline{q(x, y, t)}, \tag{19}$$

where $h = s(x, y, t) - b(x, y)$ represents the depth from the basal topography to the free surface.

In the process of depth integration, Leibnitz integral rule and the boundary conditions are exploited repeatedly to simplify the equations. Substituting the hydrostatic pressure (18) into the resulting equations, so that we obtain

$$\begin{aligned}
&\frac{\partial}{\partial t}(h\phi_f\overline{u}_f) + \frac{\partial}{\partial x}(h\phi_f\overline{u}_f\overline{u}_f) + \frac{\partial}{\partial y}(h\phi_f\overline{u}_f\overline{v}_f) \\
&\quad = -\phi_f\epsilon\frac{\partial}{\partial x}\left(\frac{1}{2}h^2\cos\zeta\right) + h\phi_f\sin\zeta - \frac{(1-\gamma)\phi_s\phi_f}{\epsilon v_T(1-\phi_s)^m}\frac{1}{\gamma}h(\overline{u}_f - \overline{u}_s) \\
&+ \frac{\epsilon}{N_R}\left[2h\frac{\partial^2\overline{u}_f}{\partial x^2} + h\frac{\partial}{\partial y}\left(\frac{\partial\overline{v}_f}{\partial x} + \frac{\partial\overline{u}_f}{\partial y}\right) - \frac{1}{\epsilon^2}\vartheta\overline{u}_f\right] - \phi_f\epsilon h\cos\zeta\frac{\partial b}{\partial x} + O(\epsilon^{1+\chi}),
\end{aligned} \tag{20}$$

$$\begin{aligned}
&\frac{\partial}{\partial t}(h\phi_f\overline{v}_f) + \frac{\partial}{\partial x}(h\phi_f\overline{u}_f\overline{v}_f) + \frac{\partial}{\partial y}(h\phi_f\overline{v}_f\overline{v}_f) \\
&\quad = -\phi_f\epsilon\frac{\partial}{\partial y}\left(\frac{1}{2}h^2\cos\zeta\right) - \frac{(1-\gamma)\phi_s\phi_f}{\epsilon v_T(1-\phi_s)^m}\frac{1}{\gamma}h(\overline{v}_f - \overline{v}_s) \\
&+ \frac{\epsilon}{N_R}\left[2h\frac{\partial^2\overline{v}_f}{\partial x^2} + h\frac{\partial}{\partial x}\left(\frac{\partial\overline{u}_f}{\partial y} + \frac{\partial\overline{v}_f}{\partial x}\right) - \frac{1}{\epsilon^2}\vartheta\overline{v}_f\right] - \phi_f\epsilon h\cos\zeta\frac{\partial b}{\partial y} + O(\epsilon^{1+\chi}),
\end{aligned} \tag{21}$$

where in the process of deriving equations (20) and (21), the blunt velocity profile is assumed. The equations (20) and (21) describe the evolutions of the fluid volume fraction ϕ_f, depth-averaged velocities $\overline{u}_f$ and $\overline{v}_f$, and the total thickness h.

4.2 Depth-Integrated for the Granular Phase

The normal component of the solid momentum equations is firstly integrated along the depth direction, and then becomes the following subject to Leibnitz

integral rule and scaling analysis,

$$\lambda\kappa h\overline{u_s^2} = -\gamma\int_b^s \frac{\partial p}{\partial z}dz - \int_b^s \cos\zeta dz + (\boldsymbol{n}_b \cdot \widetilde{\boldsymbol{T}}_s \boldsymbol{n}_b) + O(\epsilon). \tag{22}$$

Substituting the expression of the fluid pressure obtained by approximating the normal momentum equation of the fluid phase to order $O(\epsilon)$ into the equation (22), we can obtain

$$\boldsymbol{n}_b \cdot \widetilde{\boldsymbol{T}}_s \boldsymbol{n}_b = \lambda\kappa h\overline{u_s^2} - \gamma\kappa\lambda h\overline{u_f^2} - \gamma h\cos\zeta + h\cos\zeta + O(\epsilon). \tag{23}$$

To proceed, from the normal component of the solid momentum equations, the following equation can be found

$$O(\epsilon^\alpha) = -\phi_s\cos\zeta - \frac{\partial(\phi_s\widetilde{T}_{s(zz)})}{\partial z} - \phi_s\gamma\frac{\partial p}{\partial z}. \tag{24}$$

Integrating the equation (24), and substituting the fluid pressure (18), the equation (24) becomes

$$\widetilde{T}_{s(zz)} = (1-\gamma)(s-z)\cos\zeta + O(\epsilon^\alpha). \tag{25}$$

Following [3], the assumption is made that the down-slope and cross-slope normal stress vary linearly with the vertical normal stress, which is fulfilled to leading order

$$\widetilde{T}_{s(xx)} = K_x\widetilde{T}_{s(zz)} + O(\epsilon^\chi), \qquad \widetilde{T}_{s(yy)} = K_y\widetilde{T}_{s(zz)} + O(\epsilon^\chi), \tag{26}$$

where K_x and K_y are active during dilatational motion and passive during compressional motion. To avoid repeating, the derivations and expressions of K_x and K_y are not mentioned here, and can be found by referring to [3].

The down-slope and cross-slope components of the solid momentum equations are firstly integrated along the depth direction, and then Leibnitz integral rule is performed to simplify the integrated equations. Through substituting equations (18), (23), (25), and (26) into the resulting equations, the depth-integrated

equations for the granular phase finally become

$$\frac{\partial}{\partial t}(h\phi_s\overline{u}_s)+\frac{\partial}{\partial x}(h\phi_s\overline{u}_s\overline{u}_s)+\frac{\partial}{\partial y}(h\phi_s\overline{u}_s\overline{v}_s)$$
$$=h\phi_s\sin\zeta-\epsilon\phi_s\gamma\frac{\partial}{\partial x}\left(\frac{h^2\cos\zeta}{2}\right)-\epsilon\frac{\partial}{\partial x}\left(\frac{1}{2}K_x\phi_s(1-\gamma)h^2\cos\zeta\right)$$
$$+\frac{(1-\gamma)\phi_s\phi_f}{\epsilon v_T(1-\phi_s)^m}h(\overline{u}_f-\overline{u}_s)-\frac{\overline{u}_s}{|\,\overline{\boldsymbol{u}}_{\boldsymbol{s}}\,|}h\phi_s\tan\delta\left[\lambda\kappa((\overline{u}_s)^2-\gamma(\overline{u}_f)^2)+(1-\gamma)\cos\zeta\right]$$
$$-\epsilon h\phi_s\cos\zeta\frac{\partial b}{\partial x}+O(\epsilon^{(1+\chi)}), \tag{27}$$
$$\frac{\partial}{\partial t}(h\phi_s\overline{v}_s)+\frac{\partial}{\partial x}(h\phi_s\overline{u}_s\overline{v}_s)+\frac{\partial}{\partial y}(h\phi_s\overline{v}_s\overline{v}_s)$$
$$=-\epsilon\phi_s\gamma\frac{\partial}{\partial y}\left(\frac{h^2\cos\zeta}{2}\right)-\epsilon\frac{\partial}{\partial y}\left(\frac{1}{2}K_y\phi_s(1-\gamma)h^2\cos\zeta\right)$$
$$+\frac{(1-\gamma)\phi_s\phi_f}{\epsilon v_T(1-\phi_s)^m}h(\overline{v}_f-\overline{v}_s)-\frac{\overline{v}_s}{|\,\overline{\boldsymbol{u}}_{\boldsymbol{s}}\,|}h\phi_s\tan\delta\left[\lambda\kappa((\overline{u}_s)^2-\gamma(\overline{u}_f)^2)+(1-\gamma)\cos\zeta\right]$$
$$-\epsilon h\phi_s\cos\zeta\frac{\partial b}{\partial y}+O(\epsilon^{(1+\chi)}). \tag{28}$$

Besides the momentum equations, by applying the shallow assumption in the mass conservation equations, and repeating the process of depth integration, the depth-avegrated mass conservation equations can read

$$\frac{\partial(h\phi_s)}{\partial t}+\frac{\partial(h\phi_s\overline{u}_s)}{\partial x}+\frac{\partial(h\phi_s\overline{v}_s)}{\partial x}=0, \tag{29}$$
$$\frac{\partial(h\phi_f)}{\partial t}+\frac{\partial(h\phi_f\overline{u}_f)}{\partial x}+\frac{\partial(h\phi_f\overline{v}_f)}{\partial x}=0, \tag{30}$$

respectively, for the granular phase and fluid phase.

5 Numerical Investigations

In this section, numerical results of the flows of fluid-sediment mixture are presented. Referring to [10], the NOC, shocking-capture high-resolution scheme, is adopted to discretize the PDEs. The details to implement this scheme can be found in [10]. An example of debris flows with initial hemi-ellipsoidal shape down a rough inclined plane at 40° with Coulomb bed friction angle $\delta = 30°$ and merging continuously into a horizontal plane is studied. The computational domain is $x \in [0, 62]$ and $y \in [-18, 18]$ in dimensionless unit. The inclined section lies in the interval $x \in [0, 20]$ and the horizontal region lies where $x \geq 24$ with a smooth change in the topography in the transition zone, $x \in [20, 24]$. The inclination angle is prescribed by

$$\zeta(x)=\begin{cases}\zeta_0, & 0\leq x\leq 20,\\ \zeta_0(1-(x-20)/4), & 20< x <24,\\ 0°, & x\geq 24,\end{cases} \tag{31}$$

where $\zeta_0 = 40°$. The mixture is suddenly released at $t = 0$ from an ellipsoidal shell with a length of the long semi-axis $a = 4$ and that of the short semi-axis $b = 2$. The center of the cap is initially located at $(x_0, y_0) = (5, 0)$ with a maximum total height of $h^{\text{ini}}_{\text{max}} = 1$. The initial total height of the mixture is expressed as

$$h(x, y, t = 0) = h^{\text{ini}}_{\text{max}} \left(1 - \frac{(x - x_0)^2}{a^2} - \frac{(y - y_0)^2}{b^2} \right). \tag{32}$$

As the first case, the numerical results for the dry granular material ($\phi_f = 0$) flow over the defined topography is presented. The internal friction angle within the granular phase is assumed to be $\psi = 35°$. Fig. 2 demonstrates once the cap is opened, the granular mass accelerates downslope due to gravity and the body is elongated until the front reaches the horizontal run-out zone. Then, the front comes to rest due to bottom friction but the tail still accelerates further down, and the body contracts until the final deposition of the granular mass is attained.

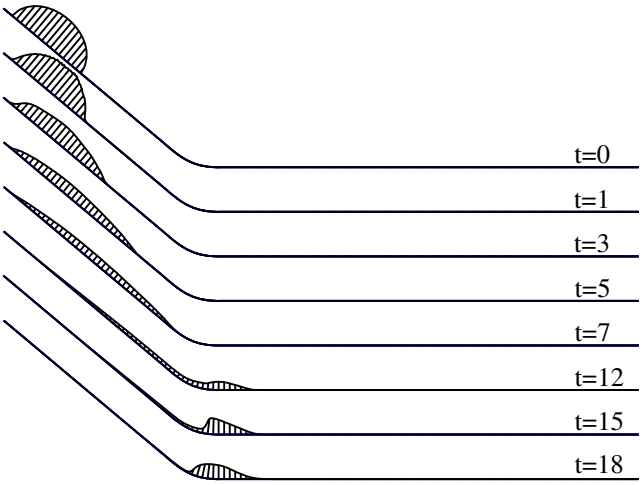

Fig. 2. The evolution for the thickness of the dry granular material along the central line of the flow for various dimensionless times

Furthermore, a general two-phase debris flow over the same topography is investigated. The densities of the fluid phase and the granular phase are chosen as $\rho_f = 1000\,\text{kg/m}^3$ and $\rho_s = 2500\,\text{kg/m}^3$, respectively. Fig. 3 shows the results for debris flow with initial homogenous fluid volume fraction $\phi_f = 0.4$. Comparing with Fig. 2, we observe that the granular phase moves faster, and the deposition is delayed in the presence of the fluid. Also, from the Fig. 3 (b), it is found that the fluid moves faster than the granular phase during the flow. This phenomenon can be explained by the fact that the Coulomb friction exerts a resistive force on

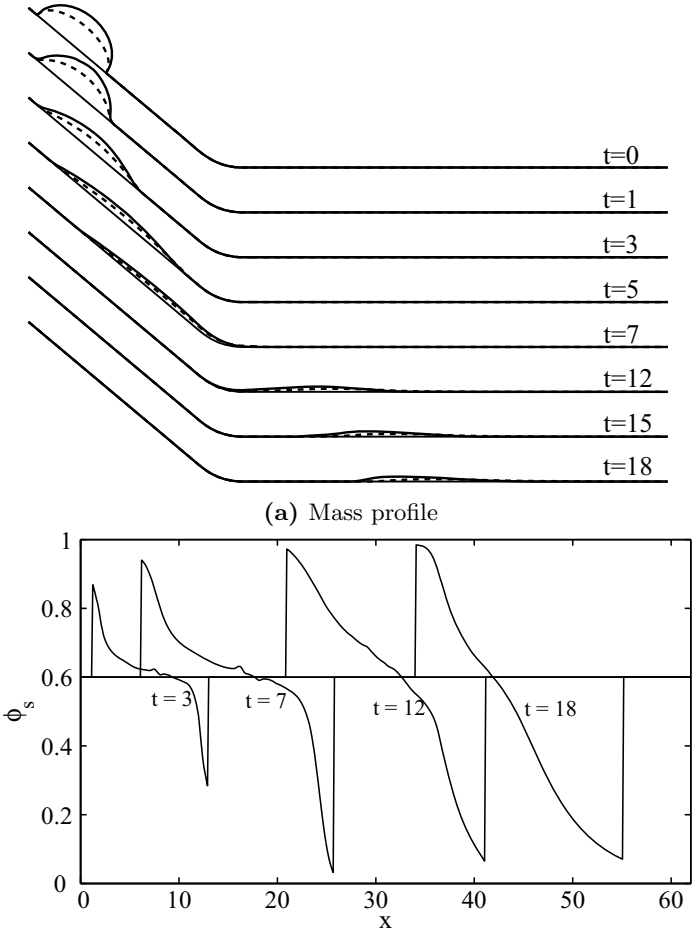

(a) Mass profile

(b) Solid volume profile

Fig. 3. Evolutions of (a) the heights of the granular phase (solid lines) and the fluid phase (dash lines), and (b) the solid volume fraction along the central line of the flow for various dimensionless times

the granular phase. A more direct overview of the debris flow can be obtained from the evolution of the three-dimensional geometries displayed in Fig. 4.

Last, another limiting suituation of the pure fluid flow ($\phi_f = 1$) is investigated, in which the depth-integrated equations are reduced to the shallow water equations. As expected, the pure fluid moves faster than dry granular material, and finally disperses completely, so that the deposition does not occur, as shown in Fig. 5.

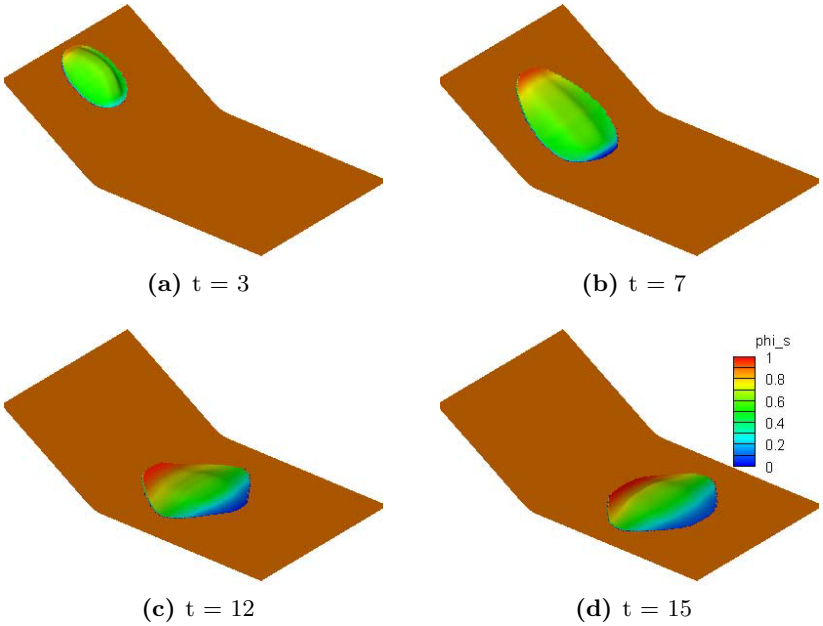

(a) t = 3 **(b)** t = 7

(c) t = 12 **(d)** t = 15

Fig. 4. Three-dimensional geometries of the debris flow at different dimensionless times $t = 3, 7, 12, 15$

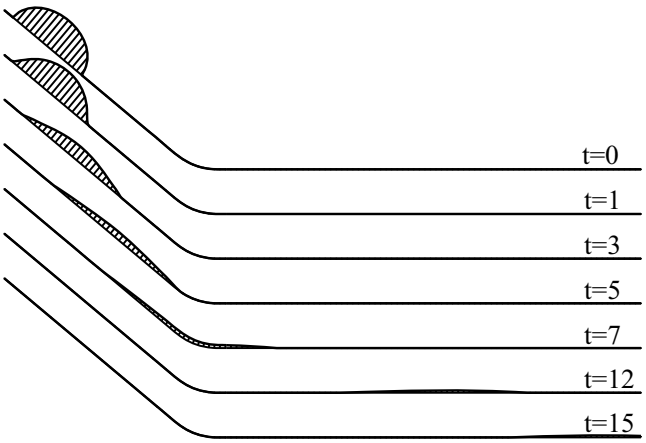

Fig. 5. The evolution of the height for pure water along the central line of the flow for various times

6 Conclusions

In the present study, a shallow two-phase model is proposed to simulate the saturated debris flows over three-dimensional shallow topography. The governing

equations are derived from the mixture theory. The resulting equations are integrated along the depth direction and simplified by shallow layer assumption. The final established equations comprise of a set of non-linear PDEs. The shocking-capture high-resolution scheme is employed to numerically solve the PDEs. Through the analysis of numerical solution, the present model can adequately describe the flows of dry granular material, general two-phase saturated debris flows and pure water. It is found that the granular phase moves faster in the presence of the fluid, and the deposition is further after flowing down an inclined surface. During the flow, the fluid phase moves faster than the granular phase, so that there are more fluid in the front of mixture. The obtained results can help the understanding of natural debris flows.

References

1. Anderson, T.B., Jackson, R.: Fluid mechanical description of fluidized beds. equations of motion. Ind. Eng. Chem. Fundam. 6, 527–539 (1967)
2. Gray, J., Wieland, M., Hutter, K.: Gravity-driven free surface flow of granular avalanches over complex basal topography. Proc. R. Soc. A 445, 1841–1874 (1999)
3. Geve, R., Koch, T., Hutter, K.: Unconfined flow of granular avalanches along a partly curved surface I. Theory. Proc. R. Soc. A 445, 399–413 (1994)
4. Pelanti, M., Bouchut, F., Mangeney, A.: A roe-type scheme for two-phase shallow granular flows over variable topography. Math. Model Numer. Anal. 42, 851–885 (2008)
5. Pitman, E.B., Le, L.: A two-fluid model for avalanche and debris flows. Phil. Trans. R. Soc. A 363, 1573–1601 (2005)
6. Pudasaini, S.P.: A general two-phase debris flow model. J. Geophys. Res. 117, 1–28 (2012)
7. Pudasaini, S.P., Wang, Y., Hutter, K.: Modelling debris flows down general channels. Nat. Hazards Earth Syst. 5, 799–819 (2005)
8. Richardson, J.F., Zaki, W.N.: Sedimentation and fluidisation: part 1. Trans. Inst. Chem. Eng. 32, 82–100 (1954)
9. Savage, S.B., Hutter, K.: The motion of a finite mass of granular material down a rough incline. J. Fluid Mech. 199, 177–215 (1989)
10. Wang, Y., Pudasaini, S.P., Hutter, K.: The Savage-Hutter theory: A system of partial differential equations for avalanche flows of snow, debris, and mud. J. App. Math. Mech. 84, 507–527 (2004)